# Demonstration of Visible Light Activated Photocatalytic Self-cleaning by Thin Films of Perovskite Tantalum and Niobium Oxynitrides

Antonio Iborra-Torres,[a] Alexander N Kulak,[b] Robert G Palgrave,[c] Geoffrey Hyett[a]*

[a] Department of Chemistry, University of Southampton, Southampton, SO17 1BJ, United Kingdom

[b] School of Chemistry, University of Leeds, Leeds, LS2 9JT, United Kingdom

[c] Christopher Ingold Laboratories, UCL, 20 Gordon Street, London, WC1H 0AJ, United Kingdom

KEYWORDS : Perovskite, oxynitride, mixed anion, photocatalysis, self-cleaning, thin film, AACVD, Chemical Vapor Deposition.

**ABSTRACT:** Metal oxynitrides adopting the perovskite structure have been shown to be visible light activated photocatalysts, and therefore have potential as self-cleaning materials, where surface organic pollutants can be removed by photomineralization. In this work, we establish a route for the deposition of thin films for seven perovskite oxynitrides, $CaTaO_2N$, $SrTaO_2N$, $BaTaO_2N$, $LaTaON_2$, $EuTaO_2N$, $SrNbO_2N$ and $LaNbON_2$, on quartz and alumina substrates using dip-coating of a polymer gel to form an amorphous oxide precursor film, followed by ammonolysis. The initially deposited oxide films were annealed at 800 °C, followed by ammonolysis at temperatures from 850 °C to 1000 °C. The perovskite oxynitride thin films were characterized using XRD and EDX, with band gaps determined using Tauc plots derived from UV-vis spectroscopic data. A cobalt oxide co-catalyst was deposited onto each film by drop casting and the photocatalytic activity assessed under visible light using dichloroindophenol dye degradation in the presence of a sacrificial oxidant. The light source used was a solar simulator equipped with a 400 nm cut-off filter. The dye degradation test demonstrated photocatalytic activity in all samples except $EuTaO_2N$ and $BaTaO_2N$. The three most active samples were $SrNbO_2N$, $CaTaO_2N$ and $SrTaO_2N$. The cobalt oxide loading was optimized for these three films and found to be 0.3 μg $cm^{-2}$. Further catalytic tests were conducted using stearic acid degradation, and this found the film of $SrNbO_2N$ with cobalt oxide co-catalyst to be the most active for complete mineralization of this model pollutant.

## INTRODUCTION

Oxynitride perovskites have been shown to be effective photocatalysts for the production of hydrogen from water – catalyzing the so-called water splitting reaction – by harvesting energy from visible light.[1-5] More recent reports have shown that perovskite oxynitrides can also photocatalytically degrade dye molecules under visible light irradiation, indicating their potential for water purification applications.[6, 7] In this paper, we explore the opportunity of using perovskite oxynitrides for visible light activated self-cleaning applications, and therefore the synthesis of these materials as thin films.

There has been widespread commercialization of titanium dioxide films in 'self-cleaning' windows where the photocatalyst coating, activated by UV light, photo-mineralizes organic species into water and carbon dioxide, and any heteroatoms into water soluble mineral acids.[8] Photocatalytic mineralization proceeds with absorption of light to form electron-hole pairs that can generate reactive oxygen species such as superoxide or hydroxide radicals by reaction with surface bound atmospheric oxygen and water. Evidence for this has been provided by quenching experiments that show that photocatalytic activity is reduced in the presence of hole and superoxide scavangers.[9, 10] The self-cleaning reaction has also been demonstrated to be able to destroy bacteria by decomposition of the cell membrane.[11, 12] Photocatalytically active titania films can also be used for air purification by removal volatile organic compounds (VOCs).[13] There would be significant commercial value in a photocatalyst coating that could demonstrate this self-cleaning and antibacterial activity but making use of the visible light available in enclosed and indoor environments.

The key requirement for a visible light activated photocatalyst is a bandgap smaller than 3 eV so that visible light photons can be absorbed, but still sufficiently large to retain band edge energies with the necessary oxidizing and reducing power to generate the reactive oxygen species required for self-cleaning.[14, 15] The perovskite oxynitrides $ABON_2$ and $LaBO_2N$, where *A* = Sr, Ba, Ca or Eu and *B* = Nb or Ta, are strongly colored compounds with visible light band gaps,[16-20] due to the presence of the more electropositive nitride ion raising the valence band maximum and decreasing the band gap relative to similar perovskite oxides .[21] Prior work on the formation of thin films of the perovskite oxynitrides has focused on magneton sputtering or pulsed laser deposition (PLD). PLD has been used for the formation of $BaTaO_2N$ and $SrTaO_2N$.[22, 23] Radio frequency

magnetron sputtering has been used for $SrTaO_2N$ and $LaNbON_2$ with substrate temperature of 300 °C to 1000 °C.[21, 24]

The perovskite oxynitrides have been investigated as water splitting visible light activated photocatalysts, with evidence of oxygen evolution from $LaTaO_2N$, $SrTaO_2N$ and $LaNbO_2N$ in the presence of silver nitrate as a sacrificial reductant.[25-27] $SrNbO_2N$ and $BaTaO_2N$ have both demonstrated overall water splitting with a platinum counter electrode under bias in photoelectrochemical experiments.[28, 29] Overall water splitting without a bias on particles of $CaTaO_2N$ has been observed.[30] For all of these examples a co-catalyst or co-catalysts were necessary.[31] Of greater relevance for self-cleaning applications powder particles of oxynitride photocatalysts have also been assessed by dye degradation tests. In these tests methyl orange was used and activity observed $SrNbO_2N$, $CaTaO_2N$ and $CaNbO_2N$. These rates were seen to increase significantly (up to a factor of 20) with the addition of a cobalt oxide co catalyst. [6, 7]

Dye degradation tests are often used as a method to establish the self-cleaning ability of a photocatalyst, or as a proxy for contaminated water sources. In these tests the photocatalyst is submerged in a solution of the dye and exposed to a light source. The degradation of the dye can be indirectly monitored by measuring the intensity of the visible absorption band of the dye. The most commonly used dye is methylene blue,[32] the degradation of which has been defined as an ISO standard test.[33] The dyes resazurin and dichloroindophenol (DCIP) have also been investigated with the advantages of faster kinetics and reduced sensitivity to re-oxidation respectively.[34] Dye tests can provide a rapid and convenient method for assessing the photocatalytic ability of a material but it should be understood that with spectroscopic monitoring full mineralization of the dye molecule is not typically being observed.[35] Instead an initial reduction or oxidation, depending on the dye, leads to conversion to a colorless form. Further oxidation can occur for full mineralization, but this is not directly observed by the loss of color in the solution. Dye tests can be considered as a necessary but not sufficient test for evidence of self-cleaning behavior. A more definitive test for thin films is the mineralization of stearic acid.[35, 36] Stearic acid is a long chain fatty acid which is a good proxy for greasy contaminants or the lipids in cell membranes, and the degradation of which can be monitored directly by infra-red spectroscopy of the C-H absorption peaks.

In this paper, we report a method for depositing adherent thin films of perovskite oxynitrides using a two-step approach; in the first stage, dip coating is used to deposit a precursor oxide film, which is then annealed under an ammonia atmosphere to yield a thin film of the oxynitride. The films can be deposited onto both alumina and quartz substrates. We demonstrate this for seven tantalum and niobium perovskite oxynitrides, which we subsequently decorate with a cobalt oxide co-catalyst. The photocatalytic ability of each thin film is established using DCIP dye tests, and the most active samples, $SrTaO_2N$, $CaTaO_2N$ and $SrNbO_2N$ are assessed using the stearic acid test, demonstrating full degradation of an organic contaminant under a visible light source.

## EXPERIMENTAL METHODS

**Thin film synthesis**. Thin films of seven perovskite oxynitrides ($ATaO_2N$, $A$ = Eu, Sr, Ba, Ca; $SrNbO_2N$; $LaNbON_2$ and $LaTaON_2$) were synthesized by ammonolysis of thin films of their respective amorphous oxide precursor, and then decorated with cobalt oxide co-catalyst nanoparticles. The oxide precursor films were prepared *via* the polymerisable complex method.[37] For this, a precursor solution was prepared by dissolving 0.89 mmol of $TaCl_5$ (Sigma-Aldrich, 99.99%), or $NbCl_5$ (Sigma-Aldrich, 99.9%), in 6.5 ml of methanol (Fisher Scientific, technical grade) and then adding a 10% molar excess of the appropriate carbonate, $Eu_2(CO_3)_3$ (Alfa Aesar, 99.99%), $CaCO_3$ (Sigma-Aldrich), $SrCO_3$ (Sigma-Aldrich, 99.9%) or $La_2(CO_3)_3$ (Sigma-Aldrich, 99.9%). Where $BaCO_3$ (Sigma-Aldrich, 99.98%) was used, a 50 % mol excess was needed to avoid formation of tantalum or niobium rich by-products. The mixtures were stirred at room temperature until complete dissolution of the precursors, after which 19.86 mmol of citric acid (Sigma-Adrich, 99.5%) and 76.8 mmol of propylene glycol (Sigma-Adrich, 99.5%) were added. The overall ratio of metal: citric acid: propylene glycol used was 1:11:43. The solution was then heated at 120 °C for 90 mins until complete evaporation of the methanol leading to the formation a transparent resin. **CAUTION: This stage leads to the evolution of toxic methanol fumes and should be carried out in a fume hood.**

For film formation, a gel of appropriate viscosity was formed by re-adding 30 wt% methanol to the resin and sonicating on an ultrasound bath for 180 seconds to ensure homogeneity. A layer of the gel was deposited onto a 25 × 25 × 1 $mm^3$ substrate using dip coating, with a 1 mm $s^{-1}$ immersion and withdrawal speed, and an immersion time of 30 seconds. The dip coating solution was 5 ml of the gel dropped onto 20 ml of tetradecafluorohexane (Sigma Aldrich, 95%). This innovative approach was developed by Ceratti *et al* so that a superficial layer of the dip-coating gel will float on the more dense but inert fluoroalkane and allow dip-coating with the minimum quantity of gel.[38] This improves the atom efficiency, and the tetradecafluorohexane can be decanted and reused. The gel-coated substrates were heated in air for 1 hour at 350 °C, 1 hour at 650 °C and finally 2 hours at 800 °C. At each stage the heating rate was 10 °C $min^{-1}$. The heating cycle converted the gel to a metal oxide thin film which was then nitrided by placing the coated substrate on a semi-circular carbon block inside a 25 mm diameter fused silica tube in a tube furnace, under a flow of ammonia gas (anhydrous, BOC). Reactions were carried out for 15 hours at temperature between 850 °C to 1000 °C depending upon the sample, with a heating rate of 3 °C and an ammonia flow rate of 250 ml $min^{-1}$. The samples were cooled down to room temperature under an ammonia atmosphere.

The substrates used were either alumina tile (Almath), or silica (UQG optics) coated with a thin layer of alumina. The alumina coating on the silica acted as a barrier layer to prevent the silica reacting with the alkali metals in the perovskite thin films, and was deposited in-house using aerosol assisted chemical vapor deposition (AACVD) using a previously reported method.[39] For this, 0.2 g of aluminum acetylacetonate (Sigma Aldrich, 99%) was dissolved in 20 ml of methanol and placed in a 50 ml three-neck round-bottom flask. A piezoelectric device was used to generate an aerosol mist of the aluminum precursor solution, which was subsequently transported into the AACVD reactor under a flow of argon gas (BOC, Pureshield).[40] The reactor temperature was set at 500 °C and the gas flow to 1 L $min^{-1}$. After deposition, the alumina-coated silica was annealed in air at 1100 °C for 10 hours with a 3 °C $min^{-1}$ heating rate.

Cobalt oxide co-catalyst particles were deposited onto the thin films, to enhance the photocatalytic rates, using a procedure modified from the literature.[41, 42] The co-catalyst concentration was studied at nominal surface concentrations of 0.04 μg $cm^{-2}$ to 0.46 μg $cm^{-2}$. To load the surface of the film with cobalt oxide co-catalyst particles a solution $4.1 \times 10^{-5}$ mol $dm^{-3}$ of $Co(NO_3)_2 \cdot 6H_2O$ in acetone was prepared, and aliquots containing the desired amount of cobalt (0.625 ml, 0.25 ml, 0.5 ml or 0.75 ml) were dropped onto the surface of the thin film. The acetone was allowed to evaporate in air, and then the samples were heated to 700 °C under a flow of 250 ml $min^{-1}$ of ammonia gas for 60 min, leading to metallic Co-nanoparticles. The active $CoO_x$ co-catalyst was obtained by mild oxidation in air at a temperature of 200 °C for 60 mins.

**Thin film characterization.** The perovskite thin films were characterized using grazing incidence x-ray diffraction (GI-XRD) collected using a Rigaku Smartlab diffractometer, operating with a rotating anode source (45 kV, 200 mA) with an incident angle of 1° across a two theta range of 10° to 80° and a step size of 0.02°, and collection times of 15 mins. Where appropriate, diffraction data were modelled using the Le Bail method, implemented in the GSAS-II software package.[43]

Diffuse reflectance data were collected from the thin films in the wavelength range 300-900 nm using a Perkin Elmer Lambda 750S spectrometer. Tauc plots were used to determine the band gaps of the perovskite films, with the absorption co-efficient determined from the film reflectivity using the Kubelka-Munk equation.[44]

SEM images were collected using a FEI Nova NanoSEM 450 FEG-SEM operating at 5 kV without coating using a CBS detector and a working distance of 5 mm. EDX mapping was carried out on the same instrument operating at 18 kV.

X-ray photoelectron spectroscopy (XPS) was carried out on a Thermo Fisher Scientific K-Alpha instrument, using Al Kα radiation (1486.6 eV) and operated in constant analyser energy mode. Samples were introduced into the vacuum chamber held at a base pressure of $5 \times 10^{-9}$ mbar, and the incident X-ray beam focused to a 400 micron spot at the sample surface, which defined the analysis area. Survey spectra and high resolution spectra were taken with pass energies of 200 eV and 50 eV respectively. Charge neutralization was carried out using a dual beam $Ar^+$ and electron flood gun. Charge correction of spectra was carried out using the adventitious C1s, which was set to a binding energy of 284.6 eV.

**Photocatalytic Analysis.** The photocatalytic ability of each the co-catalyst loaded perovskite thin films was initially assessed through decoloration of a dye in the presence of a sacrificial oxidant, with a LS0104 150W Xenon lamp solar simulator as the light source, equipped with a 400 nm cut-off filter. The dye used was 2,6-Dichloroindophenol (DCIP, Acros 98+%), and the sacrificial oxidant glycerol (Fisher, reagent grade).[34] The reaction was carried out in a double-jacketed glass vessel with water re-circulation at 15 °C in order to prevent heating of the test solution from the light source. The thin film samples were immersed in 12 ml of an aqueous solution of $5.5 \times 10^{-5}$ mol $dm^{-3}$ DCIP and $1.26 \times 10^{-2}$ mol $dm^{-3}$ glycerol, agitated by a magnetic stirrer. The radiation intensity of the solar simulator as measured at the position of the sample was 509 mW $cm^{-2}$. [**Caution: solar simulators are intense UV sources than can cause skin and eye damage**]. Dye concentration was monitored by extracting 3.5 ml aliquots of solution and recording the visible light absorption over the range 400-800 nm, using a PerkinElmer Lambda 25 spectrometer. Aliquots were then returned to the solution. Prior to starting the test, the immersed samples were kept in the dark until an equilibrium with dye adsorption had been reached, as determined by three consecutive, constant absorption measurements. Once this was achieved the solar simulator was switched on, and aliquots withdrawn at 30 min intervals up to 180 mins.

Further photocatalytic testing for the most active samples was conducted using the stearic acid degradation test.[36] Our protocol required transparent samples, so the perovskite films were deposited onto alumina-coated quartz, as detailed above. Dip-coating was then used to deposit a thin layer of stearic acid (Fisher scientific, 98%) onto the samples, from a 0.025 mol $dm^{-3}$ solution of stearic acid in dichloromethane (Immersion time of 30 s, 1 mm $s^{-1}$ withdrawal speed). IR spectra were collected over the range 3000-2800 $cm^{-1}$ using a Perkin Elmer 100 FTIR spectrometer, where 1 $cm^{-1}$ of integration of the C-H stretching bands is equivalent to $9.7 \times 10^{15}$ molecules of stearic acid.[45] A baseline measurement was recorded on the coated films and then the samples were placed under the solar simulator described above, and removed at regular intervals to recollect the IR spectra to monitor the degradation of the stearic acid layer, up to a total time of 120 mins.

## RESULTS AND DISCUSSION

**Thin film synthesis and characterization.** Seven perovskite oxynitride ($CaTaO_2N$, $SrTaO_2N$, $BaTaO_2N$, $LaTaON_2$, $EuTaO_2N$, $SrNbO_2N$ and $LaNbON_2$) were selected based on prior observation, with powder samples, of visible light activated photocatalysis. Thin films of these compositions were synthesized by ammonolysis of oxide precursor thin films, deposited onto alumina tiles.

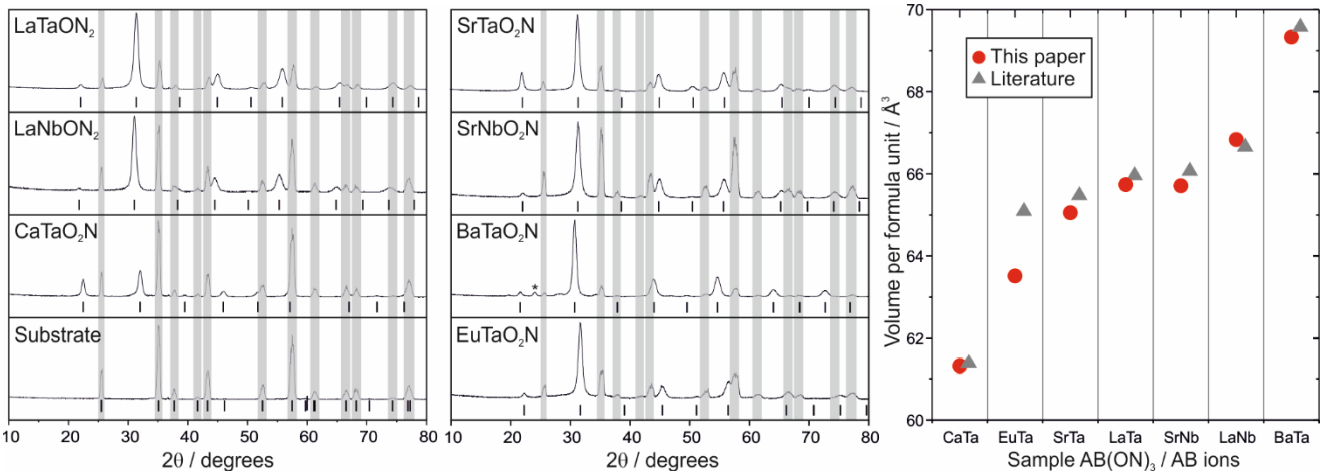


Figure 1. (Left and center) X-ray diffraction patterns of the perovskite oxynitride thin films deposited onto alumina substrates. Grey bars indicate the position of the peaks corresponding to the alumina substrate, tick marks correspond to the positions of the peaks expected for each of the perovskite phases. Asterisk (*) indicates impurity phase found in $BaTaO_2N$ film. (Right) Plot of the volume per formula unit for each of the perovskite phases, red circles labelled AB, based on the formula $AB(ON)_3$, and comparison to previously published literature values, grey triangles.

The opaque alumina substrates were used as these are inert to reaction with the perovskites at the elevated temperatures needed for ammonolysis. The oxide precursor films were deposited using dip coating from a gel made using the polymerisable complex method. In this approach, sometimes known as the citrate gel method, the desired cations are chelated with citric acid, and then a polymer is formed through condensation with glycol, thus providing an even distribution of the cations which can be maintained after dip-coating and calcination of the gel film.[37] This avoids the segregating of cations that could occur from deposition from solution due to inhomogeneous crystallization rates. After dip-coating and annealing in air the amorphous films formed in all cases were transparent and could only be observed visually on the substrate with difficulty.

Each oxide film was converted to the perovskite oxynitride through high temperature ammonolysis with a 15-hour reaction time. Ammonolysis conversion of calcined citrate gels has been successfully demonstrated in the literature for the synthesis of all of the target perovskite oxynitrides, although only as powders and not as thin films, at temperatures of 850-1000 °C.[2, 4, 19, 25, 46, 47] The ammonolysis temperature used for our thin films were adapted and optimized from the conditions previously reported. These were found to be 850 °C for $SrTaO_2N$ and $SrNbO_2N$, 950 °C for $LaNbON_2$, $EuTaO_2N$, $LaTaON_2$, and 1000 °C for $BaTaO_2N$ and $CaTaO_2N$. After ammonolysis all seven films were found to be strongly colored, ranging from straw yellow for $CaTaO_2N$, to red for $BaTaO_2N$. Photographs of the films can be found in ESI Figure S1. These oxynitride films were subsequently analyzed by GI-XRD and UV-vis spectroscopy.

In each diffraction pattern, peaks are observed which can be assigned to either the crystalline alumina phase of the substrate, or matched to database patterns of the expected perovskite oxynitride, as shown in figure 1. The diffraction patterns were modelled using a Le Bail refinement, to extract lattice parameter and particle size information for the oxynitride phase. Full Rietveld refinement could not be attempted due to the limited number of peaks present in each pattern, and the effect of the grazing incident geometry on the relative peak intensity.

The peaks originating from the alumina substrate were modelled in the $R\bar{3}c$ space group with $a$ = 5.141 Å and $\alpha$ = 55.54°. Of the oxynitride perovskites only $BaTaO_2N$ has been previously found to crystallize in the ideal cubic structure, with $Pm3m$ symmetry,[18] with the rest adopting a $I4/mcm$ tetrahedral ($SrNbO_2N$, $SrTaO_2N$,$EuTaO_2N$),[18, 46, 48] or orthorhombic distorted structure of $Imma$ ($LaTaON_2$)[48] or $Pnma$ ($CaTaO_2N$, $LaNbO_2N$),[19, 49] ignoring any possible anion ordering which cannot be detected using X-ray diffraction. These distortions are due to a tilting or twisting of the $TaO_6$ or $NbO_6$ octahedra to accommodate a smaller than ideal ion size in the 12-co-ordinate site. However, these distortions are relatively small, and require single crystal or high-resolution powder diffraction on samples with good crystallinity to be fully distinguished. As can be seen in figure 1, peak broadening prevents confirmation of the peak splitting that would identify the different symmetries. As such, when modelling the diffraction patterns we assumed that the structures adopted by the perovskite thin films were identical to those previously identified in the literature.

| Sample | Color | Band gap / eV | Space group | Vol. per formula unit / Å$^3$ | Particle ⌀/nm |
|---|---|---|---|---|---|
| $EuTaO_2N$ | Grey-Yellow | 2.48(5) | $I4/mcm$ | 63.52(6) | 71 |
| $CaTaO_2N$ | Yellow | 2.35(5) | $Pnma$ | 61.32(9) | 119 |
| $SrTaO_2N$ | Orange | 2.05(5) | $I4/mcm$ | 65.05(4) | 106 |
| $LaTaON_2$ | Orange | 2.00(5) | $Imma$ | 65.75(4) | 52 |
| $SrNbON_2$ | Orange | 1.91(5) | $I4/mcm$ | 65.71(3) | 27 |
| $BaTaO_2N$ | Red | 1.90(5) | $Pm3m$ | 69.33(2) | 796 |
| $LaNbON_2$ | Red-Brown | 1.80(5) | $Pnma$ | 66.83(2) | 99 |

**Table 1. Results of characterization for the perovskite oxynitride films deposited onto alumina.**

Using these assumptions the Le Bail refinements allowed us to model the lattice parameters and particle size broadening for the oxynitride phase of each of the thin films. Plots of the model diffraction data compared to the collected data can be found in figure S2. The *wR* values for the refinements can be found in table S1, falling in the range of 7% to 12%, which would typically indicate a relatively poor fit. However, this is mostly due to the poor fit to the alumina substrate peaks. The substrate contains very large alumina particle sizes, between 2-5 microns, which results in an unusual and difficult to fit peak shape due to a lack of powder averaging. Considering only the fit to the perovskite phase peaks in each refinement measured by the phase $R_F^2$, values of less than 5% are found indicative of a good fit between the model and the data. In each case, the models account for all of the observed Bragg peaks, with the exception of the $BaTaO_2N$ sample, where there are some small peaks due to an unassigned impurity.

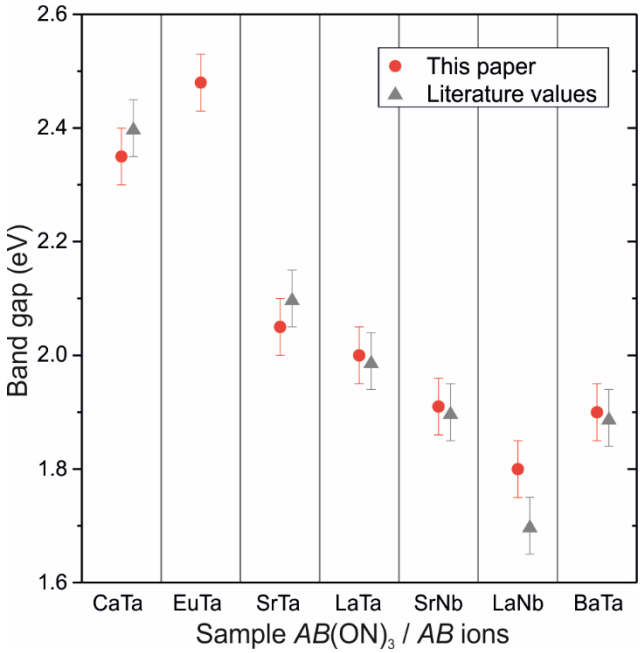


Figure 2. Plot of the band gap for each of the perovskite phases, red circles labelled AB, based on the formula $AB(ON)_3$, and comparison to previously published literature values, grey triangles.

The lattice parameters and particle size values extracted from the refinement for each of the oxynitrides are summarized in table 1. The particle size values determined from the peak broadening indicate particles of ~30-120 nm, with the exception being $BaTaO_2N$, where a much larger particle size of 800 nm is observed. There is no clear correlation between particle size and the synthesis temperature, as might be expected. In figure 1 (right hand panel) a comparison is made between the cell volume per formula unit for each sample, and the volumes previously reported in the literature. For most of the samples there is a good match between our observed cell volumes and the literature values, with a difference of less than 0.6%, indicative of successful phase formation. The exception is $EuTaO_2N$ where we observe a smaller than expected unit cell, of 2.4% by volume. $EuTaO_2N$ is a relatively underexplored material, with the literature example cited in the figure based on a fully reduced Eu(II) ion. One explanation for the smaller unit cell observed in our film would be due to increased nitridation towards $EuTaON_2$ with some oxidation of the europium to the smaller Eu(III) ion. Overall, analysis of the diffraction data suggests that films of the desired perovskite oxynitride have been formed in all cases.

The thin films were also analyzed using diffuse reflectance spectroscopy, with spectra were recorded on the films in the wavelength range of 400 – 900 nm (Figure S3), and these were used to create Tauc plots to determine the band gap (Figure S4). Based on prior literature it was assumed that the band gaps were indirect,[6] and values were found ranging from 2.48 eV for $EuTaO_2N$ down to 1.80 eV for $LaNbON_2$, as reported in table 1. In each case there is a good match, within the error of the measurement, between literature reported band gap values and the values determined from our thin films,[6, 7, 18, 19, 25, 47] as shown in figure 2. This supports the X-ray diffraction analysis in confirming the that films are composed of the target oxynitride phases. The exception to this is $EuTaO_2N$, as we were not able to identify a previously reported value for the band gap.

**Photocatalysis.** In order to initially assess the photocatalytic ability of the perovskite thin films the DCIP dye test was used,[34] alongside a cobalt oxide co-catalyst to enhance the rate of reaction.[6, 7, 41] Prior work on powders has made use of a 2 wt% loading of the co-catalyst. Assuming a 100 nm powder particle size, this equates to a particle surface loading of 0.26 μg $cm^{-2}$. In this work, the initial co-catalyst loading was similar, with a cobalt surface density 0.30 μg $cm^{-2}$.

During testing, the films were submerged in a solution of DCIP and glycerol, and irradiated with a solar simulator equipped with a 400 nm cut-off filter. DCIP is a blue dye that can undergo a two-electron transfer to a colorless form during photocatalysis with the glycerol acting as a sacrificial electron donor. This can be monitored using visible spectroscopy, assuming a Beer-Lambert law relationship between absorption and the concentration of the dye in its colored, oxidized form. Plots of the concentration of the dye as a function of time during the testing of each film can be found in figure S5.

The films of $EuTaO_2N$ and $BaTaO_2N$ showed no significant change in dye concentration over the 180 min test time, and therefore seem to be photocatalytically inactive on this timeframe, under visible light irradiation. The $CoO_x$ loaded films of $LaNbON_2$ and $LaTaON_2$ showed small reductions in dye concentration of 3% to 5% after 180 mins, indicating photocatalytic activity, while $SrTaO_2N$ effected a 9% reduction. The most active films were $CaTaO_2N$ and $SrNbO_2N$ both showed greater reductions of 26% and 46% respectively. Assuming pseudo first order kinetics with respect to the dye concentration, based on Langmuir-Hinshelwood kinetics, plots of the logarithm of the ratio of the dye concertation to the initial concentration against time

were used to determine the photocatalytic rate constants for each sample. These are shown for the active samples in figure 3, with the linear fits used to determine the first order rate constants, which can be found in table 2 for the three most active samples.

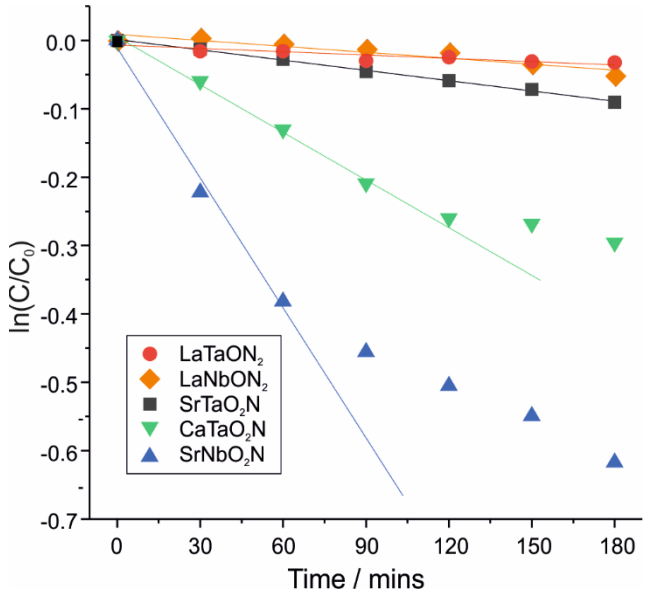


Figure 3. Plots of the ratio of dye DCIP concentration to initial concentration as a function of time for the photocatalytically active perovskite oxynitride thin films deposited on alumina, with cobalt oxide co-catalyst at a surface loading of 0.30 μg $cm^{-2}$. Tested using a solar simulator with a UV cut-off.

Relatively small 1st order rate constants of $1.6(4)\times10^{-4}$ $min^{-1}$, $2.3(5)\times10^{-4}$ $min^{-1}$ and $5.0(1)\times10^{-4}$ $min^{-1}$ are found for $LaTaON_2$, $LaNbON_2$ and $SrTaO_2N$ respectively. The two most active samples $CaTaO_2N$ and $SrNbO_2N$ have much higher initial rate constants of $24.3(5)\times10^{-4}$ $min^{-1}$ and $64(5)\times10^{-4}$ $min^{-1}$ respectively, but also show divergence away from 1st order kinetics after approximately 90 minutes, with the reactions slowing after this time. In these dye tests complete degradation of the dye is not being observed, instead the change in concentration determined from the spectra is the conversion of the dye to its colorless form. Therefore, as the reaction progresses there is an increasing concentration of the reduced colorless dye, which cannot be observed in the spectra. This by-product can still photocatalytically degrade, reducing the effective rate of decoloration of the primary dye by reducing the number of available electron-hole pairs and occupying active surface sites, explaining the reduction in rate for the two most active samples where the build-up of by-product leads to competition with the unreacted dye. The dye test is therefore a proxy rather than direct test for self-cleaning photocatalysis, but the initial 1st order rates are indicative of the relative effectiveness of the samples.

There are no clear and direct trends between the observed photocatalytic rates and any one property such as band gap, particle size, reaction temperature or structural properties. The most active sample $SrNbO_2N$ does have the smallest crystallite size and one of the smaller band gaps, which will have larger surface areas and allow for increased light absorption respectively. However, it is not clear that these factors are determinative. The two inactive samples do adopt the ideal *Pm3m* structure, whereas at least some activity is observed in the samples adopting distorted structures. This is consistent with prior work which has indicated that a local disorder or distortion is essential for an active photocatalyst, in order generate a dipole necessary to aid in separation of electron and holes.[50]

| Sample | $CaTaO_2N$ | $SrTaO_2N$ | $SrNbON_2$ |
|---|---|---|---|
| DCIP / $\times 10^{-4}$ $min^{-1}$ | 24.5(5) | 5.0(1) | 64(5) |
| Stearic Acid / $\times 10^{-4}$ $min^{-1}$ | 7.8(6) | 8(1) | 14(2) |

**Table 2. Summary 1st order rate constants for the photocatalytic dye and stearic acid tests for the most active perovskite oxynitride thin films.**

Prior work conducted by Oehler *et al* on powders using methyl orange as the test dye also found $SrNbO_2N$ followed by $CaTaO_2N$ to be the most active films, with a lesser activity for $SrTaO_2N$.[6] However our work differs from these results regarding some of the less active materials. Oehler *et al* observe a 10% reduction in dye concentration after 3 hours for methyl orange with $BaTaO_2N$, whereas we find this material to be inactive. In contrast, testing with methyl orange found $LaTaON_2$ to be inactive, while our assessment with DCIP found a small but measurable photocatalytic degradation over 3 hours. However, for the three most active materials, $SrNbO_2N$, $CaTaO_2N$ and $SrTaO_2N$ testing conducted with both methyl orange and DCIP dyes are in agreement.

For these three most active samples, further DCIP tests were conducted to confirm the ideal $CoO_x$ loading, and identify if this varied with material. Further samples of $SrNbO_2N$, $CaTaO_2N$ and $SrTaO_2N$ were prepared with targeted co-catalyst loadings of 0.04 μg $cm^{-2}$, 0.15 μg $cm^{-2}$, 0.3 μg $cm^{-2}$, and 0.46 μg $cm^{-2}$. The initial 1st order rate determined from these tests can be seen in figure 4 for each sample as a function of co-catalyst loading. This shows that for each material 0.3 μg $cm^{-2}$ is the optimum loading. Both $SrNbO_2N$ and $SrTaO_2N$ show an increase in activity with increasing loading up to this point, followed by a reduction at 0.46 μg $cm^{-2}$. $CaTaO_2N$, also shows a reduction in activity at 0.46 μg $cm^{-2}$, but also almost no activity at all below 0.3 μg $cm^{-2}$ within the error of measurement. In all cases, the presence of co-catalyst is necessary for the observation of photocatalysis, as has been previously observed,[41] as the co-catalyst can provide active centers for surface redox chemistry, and allow for surface trapping of holes and electrons, improving charge carrier separation. For the all samples a co-catalyst loading of 0.3 μg $cm^{-2}$ provided the balance between sufficient active sites without beginning to prevent light from reaching the underlying photocatalyst.

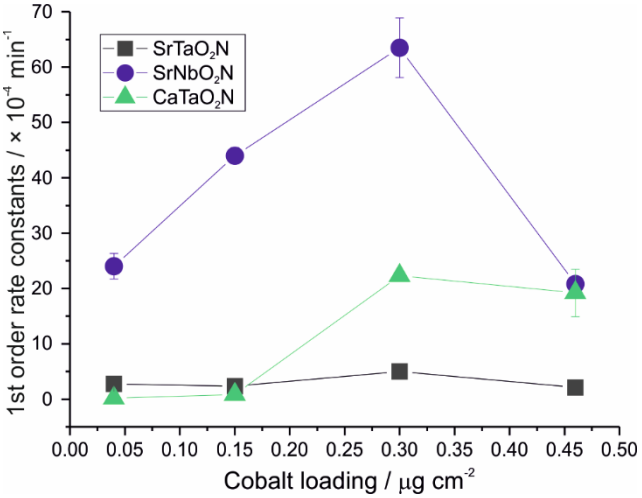


Figure 4. Plots of the initial 1st order rate constants for photocatalytic degradation of DCIP dye as a function of cobalt oxide co-catalyst loading for $SrNbO_2N$, $CaTaO_2N$ and $SrTaO_2N$ thin films on alumina substrates.

As the most active sample, the $CoO_x$ coated $SrNbO_2N$ film was further investigated using SEM and EDX mapping and XPS spectroscopy. Images of the film before the addition of the co-catalyst can be seen in Figure 5(a). In this we can see the fragmentation of the film into islands of 2-10 μm in size, due to shrinkage commonly found in films formed by dip-coating. The higher magnification images indicate that the film fragments are composed of particles on the order of 30 to 40 nm which is consistent with the crystallite size determined by XRD of 27 nm. Side-on SEM, found in S6, allows an estimation of the overall perovskite film thickness of 450-500 nm.

After deposition of the $CoO_x$ co-catalyst the morphology of the film remains unchanged, with the co-catalyst particles not observable at the resolution of the SEM. The presence of the $CoO_x$ is revealed in the EDX mapping shown in Fig 5c). This shows the regions of the sample where the strontium and niobium ions are located, corresponding to the islands seen in the SEM image, with gaps in the surface due the film shrinkage. The cobalt is detected in the EDX, and this is distributed at an even but low concentration across the surface, including in the film gaps, consistent with being deposited after the oxynitride film. The SEM/EDX therefore confirms the formation of a $SrNbO_2N$ film with a surface coverage of cobalt containing particles.

The XPS spectra allowed quantification of the surface of the film, with high resolution spectra collected for the regions where the N 1s, O 1s, Nb 3d, Sr 3d and Co 2p peaks were expected. The spectra are shown in figure S7. All five elements were observed as expected. The nitrogen 1s peak was found at a very low binding energy of 395.5 eV consistent with anionic $N^{3-}$. Both Nb 3d and Sr 3d could be modelled as single environments. The Nb $3d^{5}/_{2}$ peak was found at 206.1 eV, which lies between the values previously found for $Nb^{4+}$ and $Nb^{5+}$, based on values reported for $NbO_2$ (205.0 eV) and $Nb_2O_5$ (207.1 eV). The Sr $3d^{5}/_{2}$ peak was found at 132.9 eV, consistent with $Sr^{2+}$ in SrO. The interpretation of the Co 2p spectra was complicated by the colocation of the possible Co(II) and Co(III) peaks and near overlap with Co(0), the presence of satellite peaks for Co(II/III). Our best model suggested principally Co(II/III) with some unoxidized Co(0) remaining, approximately 6% of the Cobalt present. It is not possible to distinguish the Co(II) and Co(II) states. Interpretation of the oxygen 1s region was challenging, due to the very narrow range in which oxygen binding energies are found, and the presence of oxide in the perovskite, the cobalt co-catalyst with multiple Co oxidation states, and possible organic surface contamination. A reasonable fit to the oxygen 1s region was found by using four overlapping components with fixed FWHM, at 529.7 eV, 531.0 eV, 532.0 eV and 533.1 eV. The lowest binding energy feature was interpreted as the oxide in the perovskite where it is bound to the electropositive strontium and niobium cations. Oxide found bound to the less electropositive cobalt in the $CoO_x$ particles would be expected at a higher binding energy, interpreted as the feature at 531.0 eV. Based on the SEM images, and the 400 micron sampling size of the XPS, it is likely that some substrate alumina will be exposed, and so the peak at 532 eV can be interpreted as originating with the $Al_2O_3$ exposed in the gaps in the film seen in the SEM images, and indeed a peak is found in the survey scan where we would expect the Al 2p in an $Al_2O_3$ environment. The final oxygen 1s peak at 533.1 eV is consistent with a surface organic contaminant. Using this assignment the adjusted area of the peaks can be used to provide an approximate composition for the perovskite, relative to strontium, of $SrNb_{0.99}O_{2.48}N_{0.45}$, or $SrNb_{0.99}(O,N)_{2.93}$ This is consistent with the perovskite formula, but with some inevitable replacement of nitride by oxide, which would be expected at the very low surface depths investigated by XPS. This provides a surface oxidation state for the niobium of +4.3, which is consistent with the binding energy found for the Nb 3d peak being an intermediate oxidation state. The XPS analysis, being highly surface sensitive, gives a significant overall cobalt content. Measured relative to the strontium in the sample the surface Co:Sr ratio was found to 1:2 in atomic ratio. Assuming that the loading is 0.3 ug $cm^{-3}$ then a ratio of 1:2 would be found if the sampling depth into the film was 4.5 nm, which is consistent with XPS sampling depth of 4-7 nm.

The DCIP dye testing allowed us to identify the most active samples and the optimal co-catalyst loading. However, dye degradation is only a proxy test for self-cleaning, therefore in order to confirm the ability of the photocatalyst film to completely mineralize organic contaminants we carried out the more convincing stearic acid degradation test.[36] The protocol for stearic acid testing requires a transparent substrate, but one which is also compatible with the perovskite deposition procedure. The obvious choice is quartz, which can withstand the high temperature ammonolysis step required for the synthesis. However unlike alumina, quartz is not inert to the perovskite film and can react with the alkaline earth ions found in the oxynitrides. To overcome this challenge, a layer of aluminum oxide was first deposited onto the quartz substrate using AACVD,[39] and then the perovskite film was deposited on top of this.

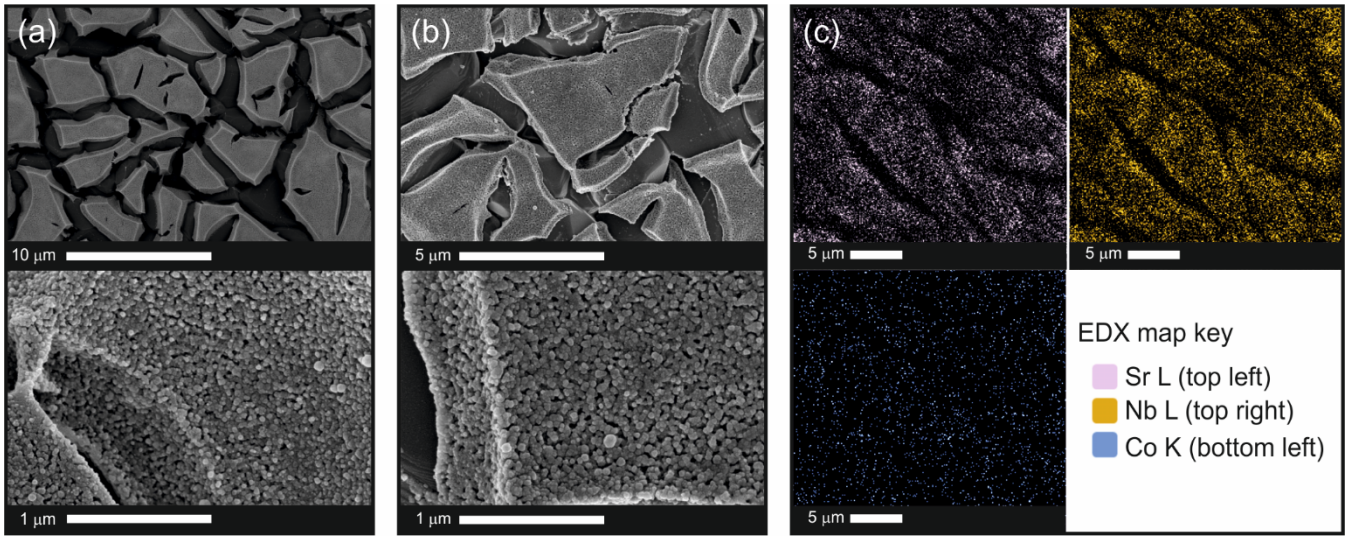


Figure 5 (a) SEM images of the $SrNbO_2N$ as deposited. (b) Images of the $SrNbO_2N$ film after deposition of $CoO_x$ co-catalyst particles at 0.3 µg $cm^{-2}$. (C) EDX mapping of the $SrNbO_2N$ sample with 0.3 µg $cm^{-2}$ of co-catalyst

This was carried out for $CaTaO_2N$, $SrNbO_2N$ and $SrTaO_2N$. PXRD was used to confirm the successful formation of these films. The diffraction patterns can be found in figure S8. UV-vis transmission spectra were also recorded, and the band gaps reconfirmed for these samples deposited on quartz as 2.43 eV, 2.15 eV, and 1.99 eV for the $CaTaO_2N$, $SrTaO_2N$ and $SrNbO_2N$ samples respectively, once again within error of values reported previously in the literature (Figure S9).

The photocatalytic test was carried out by dip-coat depositing a layer of stearic acid on to the surface of the film from a solution in dichloromethane, to give an initial concentration of approximately 1.65 $\times 10^{16}$ molecules $cm^{-2}$. The thickness of this layer was then monitored using FTIR while the samples were irradiated with UV-filtered visible light from a solar simulator for just under 2 hours, this data can be seen in figure 6. All three films show reduction in the amount of stearic acid during the experimental timeframe, of 15.4% for $SrNbO_2N$ and 8.4% for both $SrTaO_2N$ and $CaTaO_2N$, indicating that all three materials, with a co-catalyst, are capable of complete photocatalytic degradation of organic species, and can be considered truly self-cleaning coatings using visible light. The degradation of the stearic acid appears to follow 1st order kinetics and plots of $ln(C/C_0)$ against time allow for the rate constants to be determined.[51] This analysis gave a value of 14(2) $\times 10^{-4}$ $min^{-1}$ for $SrNbO_2N$, 8(1)$\times 10^{-4}$ $min^{-1}$ for $SrTaO_2N$ and 7.8(6) $\times 10^{-4}$ $min^{-1}$ for $CaTaO_2N$. In line with the results of the DCIP dye testing, $SrNbO_2N$ was the most active sample.

For the $SrNbO_2N$ thin film with a cobalt oxide co-catalyst, the initial rate of stearic acid degradation was 5.26 $\times 10^{13}$ molecules $min^{-1}$. Given the intensity of the light source used, an approximate formal quantum efficiency of 6.51 $\times 10^{-7}$ molecules per photon can be estimated. Comparing values of photocatalytic activity between different examples in the literature is challenging, because differences in experimental conditions, not all of which are reported. These can include differences in light sources used and variations in initial stearic acid film thickness that can significantly affect reported rates, and therefore such comparisons must be made with a degree of skepticism. However, having stated this, such comparison can be made with an attempt to account for differences in light intensity, assuming a linear dependence on rate. Prior work from this group under identical reaction conditions with a film of tantalum oxynitride found an initial rate 2.5 $\times 10^{13}$ molecules $min^{-1}$, or approximately half that observed with the co-catalyst loaded $SrNbO_2N$ film reported here.[52]

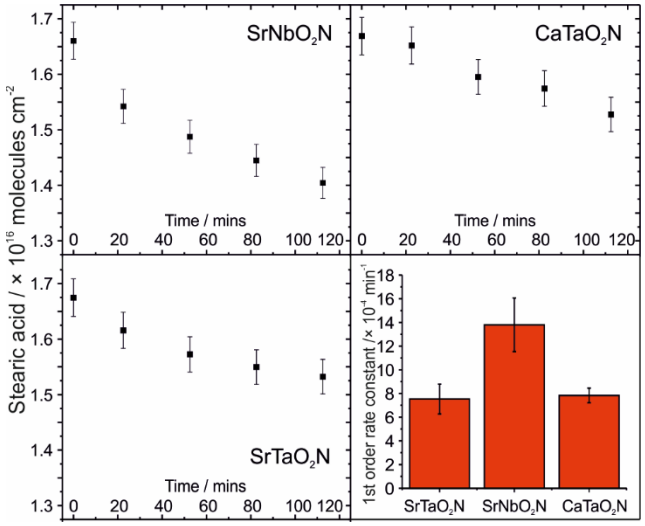


Figure 6. Plots of the stearic acid concentration as a function of time, as assessed using FTIR spectroscopy, for thin films of $SrNbO_2N$, $CaTaO_2N$ and $SrTaO_2N$ on quartz with a $CoO_x$ co-catalyst under solar simulated light. Bottom right, Plot of the 1st order rate constant for the stearic acid degradation for each film.

Prior work with visible light degradation of stearic acid on modified titanium dioxide has also been reported. Adjusting for light intensity, nitrogen doped titania films have been reported with an initial rate of 0.03 $\times 10^{13}$ molecules $min^{-1}$, while fluorinated titania films have a reported rate of

$0.2\times 10^{13}$ molecules $min^{-1}$.[53, 54] These rates are much lower than those for our perovskite oxynitride films, possibly because the low concentration of the dopants in the titania allows for only weak visible light absorption. However, more comparable rates have been observed for silver nanoparticle doped titania films, where under visible light irradiation initial photocatalytic rates for stearic acid degradant of $1.5 \times 10^{13}$ to $2 \times 10^{13}$ molecules $min^{-1}$ have been observed.[54, 56]

The initial rate identified for the best film reported here, the cobalt oxide loaded $SrNbO_2N$ film, exceeds previously reported rates for visible light photocatalytic degradation of organic species, and is certainly competitive for self-cleaning applications where visible light is the only source of radiation. We have previously estimated that a real-world loading of greasy contamination on a surface is $4 \times 10^{-6}$ g $cm^{-2}$, and that the initial rate can be used to estimate the time to completely remove this contamination under conditions of the bright sunlight, as 13.4 hours.

Comparison can also be made to UV activated titanium dioxide photocatalytic films, assuming that films are used in direct sunlight where the UV component is unfiltered. Including an adjustment again for tests conducted typically using UV light alone, and on an assumption of 5 mW $cm^{-2}$ of UV light in the solar spectrum, comparable initial rates for titania films are between $5\times 10^{13}$ and $40\times 10^{13}$ molecules $min^{-1}$ $cm^{-2}$.[57-59] It is clear that for self-cleaning applications using direct sunlight the higher rate, known non-toxicity, transparency and lower cost of $TiO_2$ make it a better choice than the films tested in this work, or other visible light activated systems currently reported in the literature. However, for situations where little UV light is available, for example for indoor applications, $CoO_x$@$SrNbO_2N$ film would be a viable self-cleaning surface.

CONCLUSION

In this paper, we have demonstrated a method for the deposition of perovskite oxynitride thin films onto both alumina and quartz substrates, and used this to form thin films of $CaTaO_2N$, $SrTaO_2N$, $BaTaO_2N$, $LaTaON_2$, $EuTaO_2N$, $SrNbO_2N$ and $LaNbON_2$. In conjunction with a cobalt oxide co-catalyst and screening using a dye degradation test, we were able to determine that films of $SrNbO_2N$ had the highest photocatalytic rate. We have determined that 0.3 μg $cm^{-2}$ is the most effective cobalt loading, and that a thin film of cobalt oxide loaded strontium niobium oxynitride is capable under visible light illumination of direct and complete degradation of stearic acid, an excellent model for organic pollutants, at a rate exceeding prior examples of visible light photocatalysts.

## ASSOCIATED CONTENT

**Supporting Information**. Figure S1 Photographs of films. S2 Rietveld refinement of films on alumina. S3 Diffuse reflectance spectra. S4 Tauc Plots. S5 Further DCIP photocatalytic data. S6 Side-on SEM image of $SrNbO_2N$ film. S7 XPS spectra collected on the $CoO_x$@$SrNbO_2N$ film. S8 Rietveld refinement of films on quartz. S9 Tauc plots of films on quartz. This material is available free of charge via the Internet at http://pubs.acs.org.

## AUTHOR INFORMATION

### Corresponding Author

*School of Chemistry, University of Southampton, Southampton, SO17 1BJ, United Kingdom. Tel (44)2380593592. E-mail: g.hyett@soton.ac.uk/

### Author Contributions

The manuscript was written through contributions of all authors.

### Funding Sources

Antonio Iborra-Torres thanks the EPSRC for provision of funding for his doctorate.

## REFERENCES

1. Maeda, K.; Domen, K., New Non-Oxide Photocatalysts Designed for Overall Water Splitting under Visible Light. *J. Phys. Chem. C.* **2007,** *111* (22), 7851-7861.
2. Higashi, M.; Abe, R.; Takata, T.; Domen, K., Photocatalytic Overall Water Splitting under Visible Light Using ATaO2N (A = Ca, Sr, Ba) and WO3 in a IO3-/I- Shuttle Redox Mediated System. *Chem. Mater.* **2009,** *21* (8), 1543-1549.
3. Kasahara, A.; Nukumizu, K.; Takata, T.; Kondo, J. N.; Hara, M.; Kobayashi, H.; Domen, K., LaTiO2N as a Visible-Light (≤600 nm)-Driven Photocatalyst (2). *The Journal of Physical Chemistry B* **2002,** *107* (3), 791-797.
4. Matoba, T.; Maeda, K.; Domen, K., Activation of BaTaO2N Photocatalyst for Enhanced Non-Sacrificial Hydrogen Evolution from Water under Visible Light by Forming a Solid Solution with BaZrO3. *Chemistry – A European Journal* **2011,** *17* (52), 14731-14735.
5. Pan, C.; Takata, T.; Nakabayashi, M.; Matsumoto, T.; Shibata, N.; Ikuhara, Y.; Domen, K., A Complex Perovskite-Type Oxynitride: The First Photocatalyst for Water Splitting Operable at up to 600 nm. *Angew. Chem. Int. Edit.* **2015,** *54* (10), 2955-2959.
6. Oehler, F.; Ebbinghaus, S. G., Photocatalytic Properties of CoOx-loaded Nano-crystalline Perovskite Oxynitrides $ABO_2N$ (A = Ca, Sr, Ba, La; B = Nb, Ta). *Solid State Sci.* **2016,** *54*, 43-48.
7. Oehler, F.; Naumann, R.; Köferstein, R.; Hesse, D.; Ebbinghaus, S. G., Photocatalytic Activity of CaTaO2N Nanocrystals Obtained from a Hydrothermally Synthesized Oxide Precursor. *Mater. Res. Bull.* **2016,** *73*, 276-283.
8. Mills, A.; Lepre, A.; Elliott, N.; Bhopal, S.; Parkin, I. P.; O'Neill, S. A., Characterisation of the Photocatalyst Pilkington Activ (TM): a Reference Film Photocatalyst? *J. Photochem. Photobiol., A* **2003,** *160* (3), 213-224.
9. Wu, D.; Wang, B.; Wang, W.; An, T.; Li, G.; Ng, T. W.; Yip, H. Y.; Xiong, C.; Lee, H. K.; Wong, P. K., Visible-Light-Driven BiOBr Nanosheets for Highly Facet-Dependent Photocatalytic Inactivation of Escherichia Coli. *Journal of Materials Chemistry A* **2015,** *3* (29), 15148-15155.
10. Ye, L.; Su, Y.; Jin, X.; Xie, H.; Zhang, C., Recent Advances in BiOX (X = Cl, Br and I) Photocatalysts: Synthesis, Modification, Facet Effects and Mechanisms. *Environmental Science: Nano* **2014,** *1* (2), 90-112.
11. Kikuchi, Y.; Sunada, K.; Iyoda, T.; Hashimoto, K.; Fujishima, A., Photocatalytic Bactericidal Effect of $TiO_2$ Thin Films: Dynamic Ciew of the Active Oxygen Species Responsible for the Effect. *J. Photochem. Photobiol., A* **1997,** *106* (1-3), 51-56.
12. Sunada, K.; Watanabe, T.; Hashimoto, K., Studies on Photokilling of Bacteria on TiO(2) Thin Film. *J. Photochem. Photobiol., A* **2003,** *156* (1-3), 227-233.

13. Peral, J.; Domènech, X.; Ollis, D. F., Heterogeneous Photocatalysis for Purification, Decontamination and Deodorization of Air. *Journal of Chemical Technology & Biotechnology* **1997,** *70* (2), 117-140.

14. Takata, T.; Tanaka, A.; Hara, M.; Kondo, J. N.; Domen, K., Recent Progress of Photocatalysts for Overall Water Splitting. *Catal. Today* **1998,** *44* (1-4), 17-26.

15. Maeda, K.; Domen, K., Photocatalytic Water Splitting: Recent Progress and Future Challenges. *The Journal of Physical Chemistry Letters* **2010,** *1* (18), 2655-2661.

16. Fuertes, A., Chemistry and Applications of Oxynitride Perovskites. *J. Mater. Chem.* *22* (8), 3293-3299.

17. Fuertes, A., Synthesis and Properties of Functional Oxynitrides - from Photocatalysts to CMR Materials. *Dalton Trans.* *39* (26), 5942-5948.

18. Kim, Y.-I.; Woodward, P. M.; Baba-Kishi, K. Z.; Tai, C. W., Characterization of the Structural, Optical, and Dielectric Properties of Oxynitride Perovskites AMO2N (A = Ba, Sr, Ca; M = Ta, Nb). *Chem. Mater.* **2004,** *16* (7), 1267-1276.

19. Logvinovich, D.; Ebbinghaus, Stefan G.; Reller, A.; Marozau, I.; Ferri, D.; Weidenkaff, A., Synthesis, Crystal Structure and Optical Properties of $LaNbON_2$ *Z. Anorg. Allg. Chem.* **2010,** *636* (6), 905-912.

20. Jansen, M.; Letschert, H. P., Inorganic Yellow-red Pigments without Toxic Metals. *Nature* **2000,** *404* (6781), 980-982.

21. Cohen, Y.; Riess, I., Preparation of Oxynitride Thin Films of $BaNb(O_yN)_x$ and $LaNb(O_yN_z)_x$ using Reactive Sputtering from Multiphase Powder Targets. *Materials Science and Engineering: B* **1994,** *25* (2), 197-202.

22. Kim, Y.-I.; Si, W.; Woodward, P. M.; Sutter, E.; Park, S.; Vogt, T., Epitaxial Thin-Film Deposition and Dielectric Properties of the Perovskite Oxynitride BaTaO2N. *Chem. Mater.* **2007,** *19* (3), 618-623.

23. Oka, D.; Hirose, Y.; Kamisaka, H.; Fukumura, T.; Sasa, K.; Ishii, S.; Matsuzaki, H.; Sato, Y.; Ikuhara, Y.; Hasegawa, T., Possible Ferroelectricity in Perovskite Oxynitride $SrTaO_2N$ Epitaxial Thin Films. *Scientific Reports* **2014,** *4*, 6.

24. Ziani, A.; Le Paven, C.; Le Gendre, L.; Marlec, F.; Benzerga, R.; Tessier, F.; Cheviré, F.; Hedhili, M. N.; Garcia-Esparza, A. T.; Melissen, S.; Sautet, P.; Le Bahers, T.; Takanabe, K., Photophysical Properties of $SrTaO_2N$ Thin Films and Influence of Anion Ordering: A Joint Theoretical and Experimental Investigation. *Chem. Mater.* **2017,** *29* (9), 3989-3998.

25. Kato, H.; Ueda, K.; Kobayashi, M.; Kakihana, M., Photocatalytic Water Oxidation under Visible Light by Valence Bband Controlled Oxynitride Solid Solutions $LaTaON_2$-$SrTiO_3$. *Journal of Materials Chemistry A* **2015,** (3), 11824-11829.

26. Wan, L. P.; Xiong, F. Q.; Zhang, B. X.; Che, R. X.; Li, Y.; Yang, M. H., Achieving Photocatalytic Water Oxidation on $LaNbON_2$ under Visible Light Irradiation. *Journal of Energy Chemistry* **2018,** *27* (2), 367-371.

27. Fu, J.; Skrabalak, S. E., Enhanced Photoactivity from Single-Crystalline SrTaO2N Nanoplates Synthesized by Topotactic Nitridation. *Angew. Chem. Int. Edit.* **2017,** *56* (45), 14169-14173.

28. Kodera, M.; Urabe, H.; Katayama, M.; Hisatomi, T.; Minegishi, T.; Domen, K., Effects of Flux Synthesis on SrNbO2N Particles for Photoelectrochemical Water splitting. *Journal of Materials Chemistry A* **2016,** *4* (20), 7658-7664.

29. Seo, J.; Nakabayashi, M.; Hisatomi, T.; Shibata, N.; Minegishi, T.; Domen, K., Solar-Driven Water Splitting over a BaTaO2N Photoanode Enhanced by Annealing in Argon. *Acs Applied Energy Materials* **2019,** *2* (8), 5777-5784.

30. Xu, J.; Pan, C.; Takata, T.; Domen, K., Photocatalytic Overall Water Splitting on the Perovskite-type Transition Metal Oxynitride CaTaO2N under Visible Light Irradiation. *Chem. Commun.* **2015,** *51* (33), 7191-7194.

31. Lu, X.; Bandara, A.; Katayama, M.; Yamakata, A.; Kubota, J.; Domen, K., Infrared Spectroscopic Study of the Potential Change at Cocatalyst Particles on Oxynitride Photocatalysts for Water Splitting by Visible Light Irradiation. *J. Phys. Chem. C* *115* (48), 23902-23907.

32. Mills, A.; Wang, J., Photobleaching of Methylene Blue Sensitised by $TiO_2$: an Ambiguous System? *J. Photochem. Photobiol., A* **1999,** *127* (1-3), 123-134.

33. Mills, A.; Hill, C.; Robertson, P. K. J., Overview of the Current ISO Tests for Photocatalytic Materials. *J. Photochem. Photobiol., A* **2012,** *237*, 7-23.

34. Mills, A.; McGrady, M., A Study of New Photocatalyst Indicator Inks. *J. Photochem. Photobiol., A* **2008,** *193* (2-3), 228-236.

35. Mills, A.; McFarlane, M., Current and Possible Future Methods of Assessing the Activities of Photocatalyst Films. *Catal. Today* **2007,** *129* (1-2), 22-28.

36. Sawunyama, P.; Jiang, L.; Fujishima, A.; Hashimoto, K., Photodecomposition of a Langmuir-Blodgett Film of Stearic Acid on $TiO_2$ Film Observed by in-situ Atomic Force Microscopy and FT-IR. *J. Phys. Chem. B* **1997,** *101* (51), 11000-11003.

37. Kakihana, M., Synthesis of high-performance Ceramics based on Polymerizable Complex Method. *J. Ceram. Soc. Jpn.* **2009,** *117* (1368), 857-862.

38. Ceratti, D. R.; Louis, B.; Paquez, X.; Faustini, M.; Grosso, D., A New Dip Coating Method to Obtain Large-Surface Coatings with a Minimum of Solution. *Adv. Mater.* **2015**, n/a-n/a.

39. Ponja, S. D.; Parkin, I. P.; Carmalt, C. J., Synthesis and Material Characterization of Amorphous and Crystalline (α-) $Al_2O_3$ via Aerosol Assisted Chemical Vapour Deposition. *RSC Advances* **2016,** *6* (105), 102956-102960.

40. Rees, K.; Lorusso, E.; Cosham, S. D.; Kulak, A. N.; Hyett, G., Combining Single Source Chemical Vapour Deposition Precursors to Explore the Phase Space of Titanium Oxynitride Thin Films. *Dalton Trans.* **2018,** *47* (31), 10536-10543.

41. Maegli, A. E.; Pokrant, S.; Hisatomi, T.; Trottmann, M.; Domen, K.; Weidenkaff, A., Enhancement of Photocatalytic Water Oxidation by the Morphological Control of LaTiO2N and Cobalt Oxide Catalysts. *The Journal of Physical Chemistry C* **2014,** *118* (30), 16344-16351.

42. Zhang, F.; Yamakata, A.; Maeda, K.; Moriya, Y.; Takata, T.; Kubota, J.; Teshima, K.; Oishi, S.; Domen, K., Cobalt-Modified Porous Single-Crystalline $LaTiO_2N$ for Highly Efficient Water Oxidation under Visible Light. *J. Am. Chem. Soc.* **2012,** *134* (20), 8348-8351.

43. Toby, B. H.; Von Dreele, R. B., GSAS-II: the Genesis of a Modern Open-source All Purpose Crystallography Software Package. *J. Appl. Crystallogr.* **2013,** *46*, 544-549.

44. Tauc, J., Optical Properties and Electronic Structure of Amorphous. *Mater. Res. Bull.* **1968,** *3* (1), 37-&.

45. Mills, A.; Wang, J., Simultaneous Monitoring of the Destruction of Stearic Acid and Generation of Carbon Dioxide by Self-Cleaning Semiconductor Photocatalytic Films. *J. Photochem. Photobiol., A* **2006,** *182* (2), 181-186.

46. Motohashi, T.; Hamade, Y.; Masubuchi, Y.; Takeda, T.; Murai, K.-i.; Yoshiasa, A.; Kikkawa, S., Structural Phase Transition in the Perovskite-type Tantalum Oxynitrides, $Ca_{1-x}Eu_xTa(O,N)_3$. *Mater. Res. Bull.* **2009,** *44* (9), 1899-1905.

47. Siritanaratkul, B.; Maeda, K.; Hisatomi, T.; Domen, K., Synthesis and Photocatalytic Activity of Perovskite Niobium Oxynitrides with Wide Visible-Light Absorption Bands. *ChemSusChem* **2011,** *4* (1), 74-78.

48. Clark, L.; Oró-Solé, J.; Knight, K. S.; Fuertes, A.; Attfield, J. P., Thermally Robust Anion-Chain Order in Oxynitride Perovskites. *Chem. Mater.* **2013,** *25* (24), 5004-5011.

49. Gunther, E.; Hagenmayer, R.; Jansen, M., Structural Investigations on the Oxidenitrides $SrTaO_2N$, $CaTaO_2N$ and $LaTaON_2$ by Neutron and X-ray Powder Diffraction. *Z. Anorg. Allg. Chem.* **2000,** *626* (7), 1519-1525.

50. Inoue, Y., Photocatalytic Water Splitting by $RuO_2$-Loaded Metal Oxides and Nitrides with $d^0$- and $d^{10}$ -Related Electronic Configurations. *Energy & Env. Sci.* **2009,** *2* (4), 364-386.

51. Ghazzal, M. N.; Barthen, N.; Chaoui, N., Photodegradation kinetics of stearic acid on UV-irradiated Titania Thin Film Separately Followed by Optical Microscopy and Fourier Transform Infrared Spectroscopy. *Applied Catalysis B: Environmental* **2011,** *103* (1), 85-90.

52. Cosham, S. D.; Celorrio, V.; Kulak, A. N.; Hyett, G., Observation of Visible Light Activated Photocatalytic Degradation of Stearic Acid on Thin Films of Tantalum Oxynitride Synthesized by Aerosol Assisted Chemical Vapour Deposition. *Dalton Trans.* **2019,** *48* (28), 10619-10627.

53. Quesada-Cabrera, R.; Sotelo-Vázquez, C.; Quesada-González, M.; Melián, E. P.; Chadwick, N.; Parkin, I. P., On the Apparent Visible-Light and Enhanced UV-Light Photocatalytic Activity of Nitrogen-Doped $Tio_2$ Thin Films. *J. Photochem. Photobiol., A* **2017,** *333*, 49-55.

54. Park, J. S.; Choi, W., Enhanced Remote Photocatalytic Oxidation on Surface-Fluorinated $TiO_2$. *Langmuir* **2004,** *20* (26), 11523-11527.

55. Dunnill, C. W.; Page, K.; Aiken, Z. A.; Noimark, S.; Hyett, G.; Kafizas, A.; Pratten, J.; Wilson, M.; Parkin, I. P., Nanoparticulate Silver Coated-Titania Thin Films—Photo-Oxidative Destruction of Stearic Acid under Different Light Sources and Antimicrobial Effects under Hospital Lighting Conditions. *J. Photochem. Photobiol., A* **2011,** *220* (2), 113-123.

56. Kafizas, A.; Kellici, S.; Darr, J. A.; Parkin, I. P., Titanium Dioxide snd Composite Metal/Metal Oxide Titania Thin Films on Glass: A Comparative Study of Photocatalytic Activity. *J. Photochem. Photobiol., A* **2009,** *204* (2), 183-190.

57. Quesada-Cabrera, R.; Sotelo-Vazquez, C.; Darr, J. A.; Parkin, I. P., Critical Influence of Surface Nitrogen Species on The Activity of N-Doped $Tio_2$ Thin-Films During Photodegradation of Stearic Acid Under UV Light Irradiation. *Applied Catalysis B: Environmental* **2014,** *160–161*, 582-588.

58. Platt, N. J.; Kaye, K. M.; Limburn, G. J.; Cosham, S. D.; Kulak, A. N.; Palgrave, R. G.; Hyett, G., Order of Magnitude Increase in Photocatalytic Rate for Hierarchically Porous Anatase Thin Films Synthesized from Zinc Titanate Coatings. *Dalton Trans.* **2017,** *46* (6), 1975-1985.

59. Pore, V.; Rahtu, A.; Leskelä, M.; Ritala, M.; Sajavaara, T.; Keinonen, J., Atomic Layer Deposition of Photocatalytic $TiO_2$ Thin Films from Titanium Tetramethoxide and Water. *Chem. Vap. Deposition* **2004,** *10* (3), 143-148.